PROCEEDINGS OF SCIENCE

ONLINE ICRC 2021
THE ASTROPARTICLE PHYSICS CONFERENCE
Berlin | Germany
37th International Cosmic Ray Conference
12–23 July 2021

The performance of the LHAASO-KM2A tested by the cosmic-ray Moon shadow

Yuncheng Nan[a,b,*], **Zhe Li**[b], **Songzhan Chen**[b], **Cunfeng Feng**[a], **Sha Wu**[b], **Yizhuo Li**[b]
on behalf of the LHAASO Collaboration
(a complete list of authors can be found at the end of the proceedings)

[a] *Shandong University, Institute of Frontier and Interdisciplinary Science, 72, Binhai Road, Jimo, Qingdao, Shandong, China*

[b] *Key Laboratory of Particle Astrophysics, Institute of High Energy Physics, CAS, 19-yi, Yuquan Road, Shijingshan District, Beijing, China*

E-mail: nanyc@ihep.ac.cn

The KM2A is a major ground-based array for the researches on cosmic rays around the "knee" region and the ultra high energy gamma-ray astronomy, which depends heavily on its performance. The half array of the KM2A has been operated from December 27, 2019 to November 30, 2020. The cosmic ray Moon shadow, which moves between ±25° of declination and is observed with significance up to -25 standard deviation each month, is used as an unique and powerful source to test the array's performance. Through the observation of the characteristics of the Moon shadow, including the position displacement, shape, deficit, and their variation with the time and energy, we test the pointing error, angular resolution, long-term stability of the KM2A and the absolute energy scale of the primary cosmic-ray particles. In particular, the pointing errors for showers from different declinations are discussed in this work.

**** 37th International Cosmic Ray Conference (ICRC2021), ****
**** 12-23 July 2021 ****
**** Berlin, Germany - Online ****

PoS(ICRC2021)350

1. Introduction

Cosmic rays are high energy particles from outside the solar system. The main components of cosmic rays are positive charged nuclei. These nuclei usually arrive at the Earth nearly isotropically. When they travel in the universe before arriving at Earth, they may be blocked by the Moon. In 1957, Clark proposed the loss of intensity of the cosmic rays in the direction of the Moon, the so-called Moon shadow, might provide information about the magnetic field between Moon and Earth[1].

In the past 30 years, Moon shadow has been observed by many extensive atmospheric shower(EAS) experiments, even muon and neutrino experiments, such as CYGNUS, Tibet ASγ, CASA, Milagro, ARGO-YBJ, HAWC, MACRO, Sudan-2, and ANTARES, etc. The observation of the Moon shadow can provide unique information on the experiment performances, including pointing and angular resolution. In addition, charged particles are deflected by Lorentz force in the geomagnetic field which direction is about from south to north. And this deflection is depending on the rigidity. The displacement of the Moon shadow along the east-west direction has been used to determine the absolute energy scale of the primary cosmic-ray particles by Tibet ASγ[2], ARGO-YBJ[3] and so on. Because of the Moon's circular motion each month, these features of Moon shadow can be used to detect the long-term stability of the experiments[2][3].

The Large High Altitude Air Shower Observatory (LHAASO) is a new-generation complex EAS array being constructed at Daocheng, Sichuan province, China (100.01^{o}E, 29.35^{o}N). It is composed of three sub-arrays, including the one square-km array (KM2A), Water Cherenkov Detector Array (WCDA), and the wide-field air Cherenkov/fluorescence telescopes (WFCTA) array[4]. The main goals of LHAASO include the researches on cosmic rays and gamma-ray astronomy[5]. With the half of KM2A operated since the end of 2019, Crab Nebula has been observed as the standard candle to check the detector performance[6] and 12 ultra high energy gamma-ray source are revealed[7].

According to the results of Crab, we have demonstrated the performance of half of km2a for gamma-rays, but the observation performance for charged nuclei is not known clearly. On the other hand, the position of Crab is fixed in the equatorial coordinate system, and it is not enough for the detector to detect the source on other declination bands. The motion of Moon shadow is between about $\pm 25^o$ of declination. Therefore, it is necessary to further test the performance of the array for sources at different declinations. In this work, we will analyze the Moon shadow observed by the half of KM2A using the data from December 27, 2019 to November 30, 2020. The pointing error, the angular resolution, the long-term stability of the half array of KM2A, and the absolute energy scale of the primary cosmic-ray particles are discussed in detail.

2. The LHAASO-KM2A

The half of KM2A includes 2365 electromagnetic particle detectors(EDs) and 578 muon detectors(MDs). The EDs are distributed with a spacing of 15 m, and the MDs are distributed with a spacing of 30 m. Through detecting the number of secondary particles and their arriving time, EDs are used to reconstruct the direction, core location and energy of showers. More details about the detector can be found in [4]. The half array has been successfully operated from November 2019

to December 2020. The data is collected, triggered, calibrated, selected, and reconstructed through a standard pipeline. More details about the process can be found in [6]. The average duty cycle is higher than 90%. The simulation data, mainly protons, are generated by the air shower simulation software CORSIKA (version 7.6400) and the detector response software G4KM2A[8]. The energy is from 1 TeV to 10 PeV and the zenith angle is sampled from 0^o to 70^o. These simulation sample are used for the simulation for the Moon shadow and estimation of the performance of the detectors.

3. Data analysis

The data are analyzed under following conditions: (1) The Moon is rotating around the earth at all times, therefore the observation of the Moon shadow may overlap with the Sun shadow. The distance between these two sources need to be more than 5^o. (2)Zenith angle less than 50^o.

The data set is divided into 9 groups according to N_{fit} (the number of fired EDs after filtering out the noise) which is related to the energy of the primary particle: (1)13~23; (2)23~38; (3)38~58; (4)58~86; (5)86~123; (6)123~172; (7)172~234; (8)234~315; (9)315~417.

For each data set, the $20^o \times 20^o$ sky map in celestial coordinates (right ascension RA and declination Dec.) is built with $0.1^o \times 0.1^o$ bin size. Fixing the (0, 0) of the map at the center of the Moon, the number of the observed events in each bin is recorded to the N_{on}. The corresponding background in each bin is estimated by the direct integral method which is used in the crab paper [6] where we called it N_b. The background events are subtracted from the total observed events to obtain the signal events N_s. Then we calculated the statistical significance of these signals by the $Li\&Ma'$s formula(9)[9] with taking into account the angular resolution.

The position and shape information of the Moon shadow is obtained by 1D projection of the sky map of the signal events N_s. Gaussian fitting is used to get the peak position of and width of the distribution, namely mean value and RMS value. According to the results from Tibet ASγ[2] and ARGO-YBJ[3], as well as the simulation[10], the Earth's magnetic field near the north-south direction will not make the Moon shadow move in the north-south direction, so the position of Moon shadow in the north-south direction can represents the pointing accuracy. According to the simulation results, the RMS value can be approximately calculated by the formula:

$$RMS = \sigma\sqrt{1 + (\frac{R_{Moon}}{2\sigma})^2}, \tag{1}$$

where R_{Moon} and σ represent the Moon radius and the angular resolution. Similarly, we can calculate the position of the Moon shadow in the east-west direction. According to the simulation calculation, affected by the geomagnetic field on the Lorentz force deflection of cosmic rays, the average deflection of particles satisfies the formula:

$$\delta\theta = 1.6^o \times \frac{Z}{E[TeV]}, \tag{2}$$

where E and Z represent energy and charge number respectively. Therefore, with the increase of N_{fit}, the displacement of the Moon shadow in the east-west direction also decreases and finally tends to be stable. The absolute energy scale of the primary particles can be obtained by the relationship between displacement and N_{fit}, and the minimum displacement can give the pointing accuracy of the detectors in the east-west direction.

4. Result and discussion

4.1 Pointing accuracy

The pointing accuracy of the detector is related to the establishment of the horizontal coordinate system of the experiment. The geographic location of the horizontal coordinate system and the experiment is Xian Geodetic Coordinate System 1980, China. After transformation, it is connected with the equatorial coordinate system to definite the horizontal coordinate system of the experiment. To verify the accuracy of the definition of the horizontal coordinate system, the positions of the Moon shadows observed from the east and west direction of the detector array are explored, as shown in Figure 1.

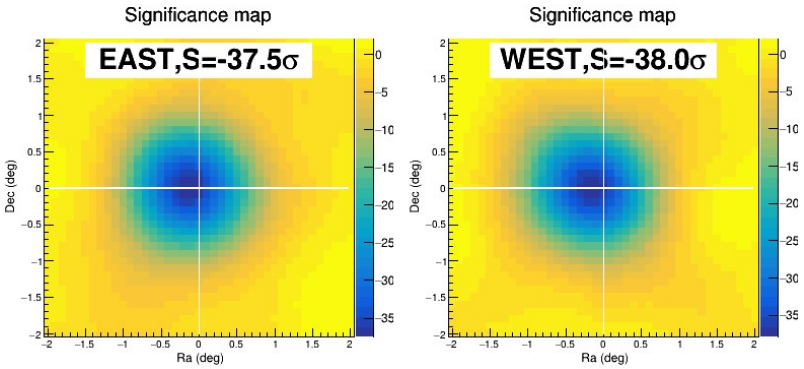

Figure 1: The significance maps of the Moon shadow from the east(left plot) and the west(right), respectively. The range of the zenith angle is from 20^o to 50^o, and nine data sets (different N_{fit}) are involved.

We can see that the significances of the Moon shadow observed from the east and west direction of the detector array are about -38σ. The position of the Moon shadow from the east is $(-0.14^o \pm 0.02^o, 0.01^o \pm 0.02^o)$ and the position of the Moon shadow from the west is $(-0.16^o \pm 0.02^o, 0.00^o \pm 0.02^o)$. From the results, it can be seen that the Moon shadow observed in the east and west direction of the array is approximately the same, so the definition of the array horizon coordinate system is correct.

The pointing accuracy of the detector is related to the detector coordinates, time calibration, direction reconstruction method, etc. By measuring the Moon shadow under different zenith angles, the correctness and accuracy of the above three points can be verified. Through fitting analysis, we calculated the position of the Moon shadow, as shown in Figure 2.

It can be seen that under different zenith angles, the north-south displacement of the Moon shadow are consistent within the error range. More specifically, we use the constant function to fit the size of the total displacement under different zenith angles, as shown as P_o in Figure 2, which is consistent with the fitting results in Figure 1. The initial accuracy of the detector coordinates, time calibration, and direction reconstruction method are verified.

In addition, we also calculate the displacement of the Moon shadow in the north-south direction under different N_{fit} to give the pointing accuracy of the detector in the north-south direction, as shown in the left plot in Figure 3. The displacement of the Moon shadow in the north-south direction does not change with the increase of N_{fit}, which is the same in the error range. Through

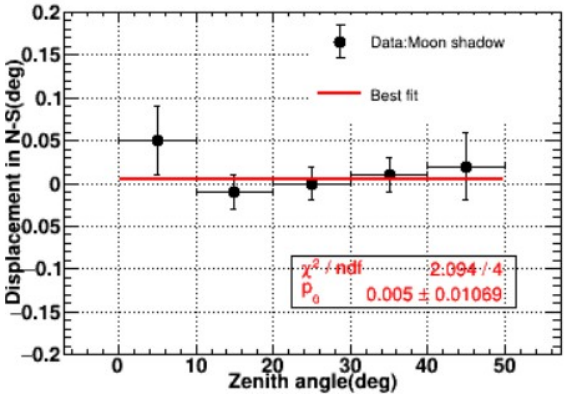

Figure 2: The displacement of the Moon shadow for different zenith angles along the north and south direction. Nine data sets (different N_{fit}) are involved.

the constant function to fit the size of the overall displacement under different N_{fit}, the north-south pointing accuracy of the array is $0.02^o \pm 0.01^o$.

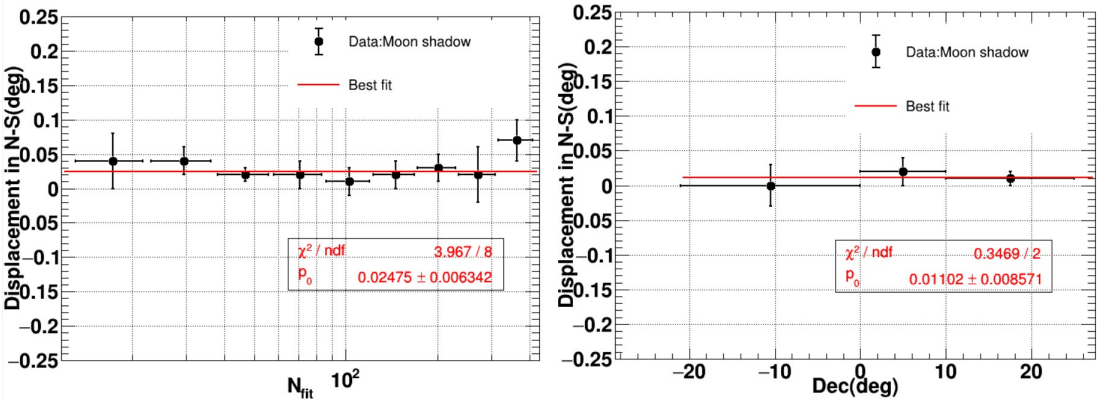

Figure 3: The displacement of the Moon shadow for different N_{fit} along the north and south direction(left plot) and it's change for different declinations(right).

Considering that the detector can survey the sky in the declination band from -15^o to 75^o, for different declination, the point accuracy of the detector may be different. In order to explore this point, we calculate the displacement of the Moon shadow under different declinations to give the pointing accuracy of the north and south of the array, as shown in the right plot in Figure 3. It can be seen from the figure that the displacement of the Moon shadow in the north-south direction does not change with the change of declination, which is very stable. We also use the constant function to fit the total displacement size under different declination and get the total north-south displacement direction of the array is $0.01^o \pm 0.01^o$. In conclusion, the accuracy of declination obtained by the detector for different sources is stable.

4.2 Angular resolution

With the change of N_{fit}, the angular resolution of the detector can be obtained by the fitting of the Moon shadow and then calculated by formula 1. The result is shown in Figure 4. This result

is in agreement with the angular resolution obtained by the simulation data, but a slight difference, which may come from the single component of the simulated primary particles.

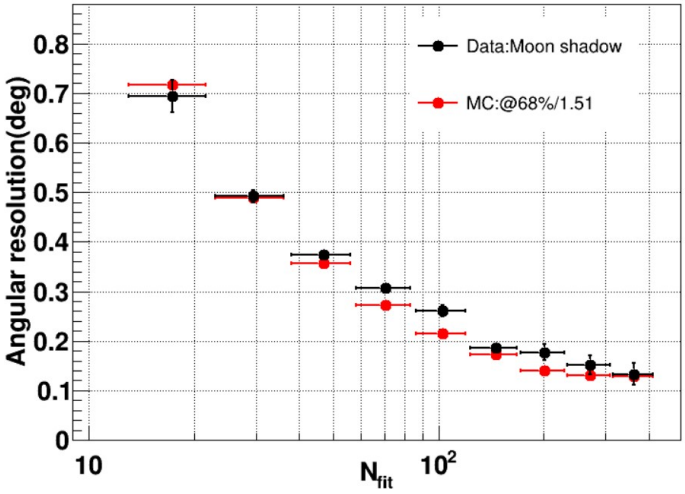

Figure 4: The angular resolution at different N_{fit} obtained from the Moon shadow and the simulation.

4.3 Absolute energy scale

We explored the displacement of the Moon shadow along the east and west direction under different N_{fit}, as shown in Figure 5. As N_{fit} increases, the displacement decreases. We use $k \times {N_{fit}}^{\lambda}$to fit this change and get $k = -0.60 \pm 0.19$, and $\lambda = 0.36 \pm 0.08$. More research on the absolute energy scale will be carried out in the future.

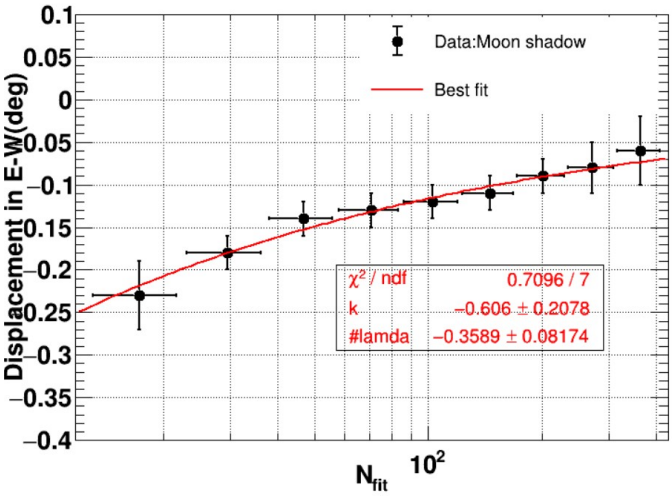

Figure 5: The displacement of the Moon shadow for different N_{fit} along the east and west direction.

4.4 Long-term stability of detector

In order to explore the long-term stability of the array, we monitored the position and angular resolution of the Moon shadow every month. The results are summarized in Figure 6. We can see that the data is stable for different months within the error range of nearly 1σ.

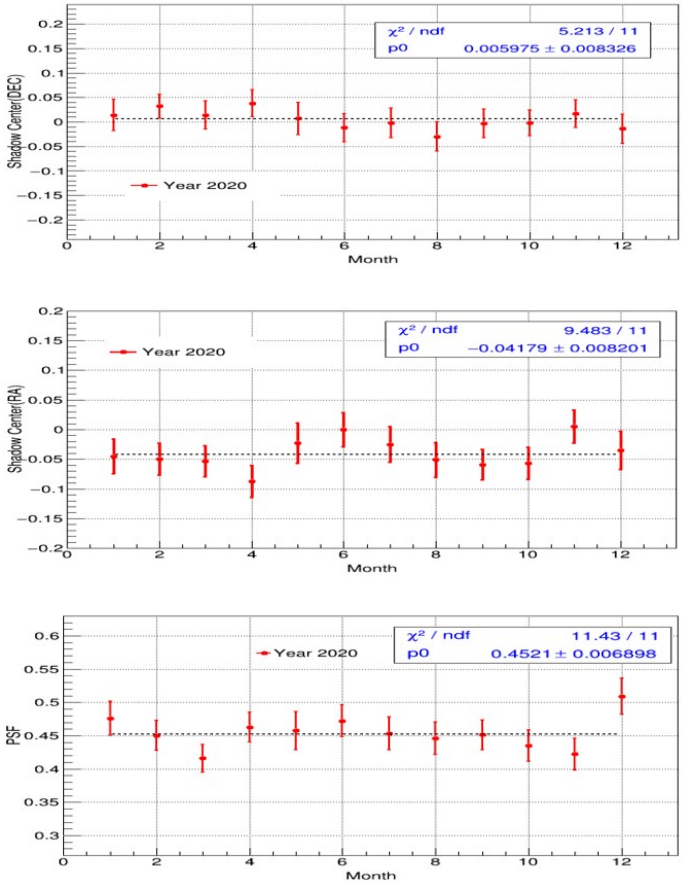

Figure 6: The variation of the declinations, the right ascensions, and the angular resolution of Moon shadow with month.

5. Conclusion

Using the data of the half of KM2A, the Moon shadow is observed to investigate the performance of the detectors. The pointing error is $0.02^o \pm 0.01^o$. The angular resolution from the Moon shadow is in agreement with that from the simulation. The relationship between the displacement of the Moon shadow along the east and west direction and N_{fit} is also calculated to satisfy $(-0.60 \pm 0.19) \times {N_{fit}}^{(0.36\pm0.08)}$. Through monitoring the position of the Moon shadow, and the angular resolution variance as time goes by, we find the detector is very stable. Besides, we find that the accuracy of the detector for the position of the source on different declination bands is the same. In the future, the simulation of the Moon shadow will be involved and the absolute energy scale of the primary particle will be investigated.

6. Acknowledge

This work is supported by the National Key R&D Program of China (No. 2018YFA0404201) and the Natural Sciences Foundation of China (No. 11575203 and No. 11775131).

References

[1] G. W. Clark, 1957, Phys. Rev. 108, 450

[2] M. Amenomori, X. J. Bi et al, 2009, ApJ, 692, 61

[3] B. Bartoli, P. Bernardini et al, 2011, PRD, 84, 022003

[4] H. H. He, 2018, Radiation Detection Technology and Methods, 2, 7

[5] Z. Cao, 2010, Chin. Phys. C, 34, 249

[6] F. A. Aharonian, Z. Cao, 2021, Chin. Phys. C, 45, 025002

[7] Z. Cao, F. A. Aharonian, 2021, Nature, 594, 33

[8] S. Z. Chen, C. Jin, Z. Li, 2019, 36nd International Cosmic Ray Conference

[9] T. P. Li, Y. Q. Ma, 1983, ApJ, 272, 317

[10] Y. C. Nan, S. Z. Chen, 2019, 36nd International Cosmic Ray Conference

Full Authors List: LHAASO Collaboration

Zhen Cao[1,2,3], F. Aharonian[4,5], Q. An[6,7], Axikegu[8], L.X. Bai[9], Y.X. Bai[1,3], L.X. Bai[9], Y.X. Bai[1,3], Y.W. Bao[10], D. Bastieri[11], X.J. Bi[1,2,3], Y.J. Bi[1,3], H. Cai[12], J.T. Cai[11], Zhe Cao[6,7], J. Chang[13], J.F. Chang[1,3,6], B.M. Chen[14], E.S. Chen[1,2,3], J. Chen[9], Liang Chen[1,2,3], Liang Chen[15], Long Chen[8], M.J. Chen[1,3], M.L. Chen[1,3,6], Q.H. Chen[8], S.H. Chen[1,2,3], S.Z. Chen[1,3], T.L. Chen[16],X.L. Chen[1,2,3], Y. Chen[10], N. Cheng[1,3], Y.D. Cheng[1,3], S.W. Cui[14], X.H. Cui[17], Y.D. Cui[18], B. D'Ettorre Piazzoli[19], B.Z. Dai[20], H.L. Dai[1,3,6], Z.G. Dai[7], Danzengluobu[16], D. della Volpe[21], X.J. Dong[1,3], K.K. Duan[13], J.H. Fan[11], Y.Z. Fan[13], Z.X. Fan[1,3], J. Fang[20], K. Fang[1,3], C.F. Feng[22], L. Feng[13], S.H. Feng[1,3], Y.L. Feng[13], B. Gao[1,3], C.D. Gao[22], L.Q. Gao[1,2,3], Q. Gao[16], W. Gao[22], M.M. Ge[20], L.S. Geng[1,3], G.H. Gong[23], Q.B. Gou[1,3], M.H. Gu[1,3,6], F.L. Guo[15], J.G. Guo[1,2,3], X.L. Guo[8], Y.Q. Guo[1,3], Y.Y. Guo[1,2,3,13], Y.A. Han[24], H.H. He[1,2,3], H.N. He[13], J.C. He[1,2,3], S.L. He[11], X.B. He[18], Y. He[8], M. Heller[21], Y.K. Hor[18], C. Hou[1,3], H.B. Hu[1,2,3], S. Hu[9], S.C. Hu[1,2,3], X.J. Hu[23], D.H. Huang[8], Q.L. Huang[1,3], W.H. Huang[22], X.T. Huang[22], X.Y. Huang[13], Z.C. Huang[8], F. Ji[1,3], X.L. Ji[1,3,6], H.Y. Jia[8], K. Jiang[6,7], Z.J. Jiang[20], C. Jin[1,2,3], T. Ke[1,3], D. Kuleshov[25], K. Levochkin[25], B.B. Li[14], Cheng Li[6,7], Cong Li[1,3], F. Li[1,3,6], H.B. Li[1,3], H.C. Li[1,3], H.Y. Li[7,13], J. Li[1,3,6], K. Li[1,3], W.L. Li[22], X.R. Li[1,3], Xin Li[6,7], Xin Li[8], Y. Li[9], Y.Z. Li[1,2,3], Zhe Li[1,3], Zhuo Li[26], E.W. Liang[27], Y.F. Liang[27], S.J. Lin[18], B. Liu[7], C. Liu[1,3], D. Liu[22], H. Liu[8], H.D. Liu[24], J. Liu[1,3], J.L. Liu[28], J.S. Liu[18], J.Y. Liu[1,3], M.Y. Liu[16], R.Y. Liu[10], S.M. Liu[8], W. Liu[1,3], Y. Liu[11], Y.N. Liu[23], Z.X. Liu[9], W.J. Long[8], R. Lu[20], H.K. Lv[1,3], B.Q. Ma[26], L.L. Ma[1,3], X.H. Ma[1,3], J.R. Mao[29], A. Masood[8], Z. Min[1,3], W. Mitthumsiri[30], T. Montaruli[21], Y.C. Nan[22], B.Y. Pang[8], P. Pattarakijwanich[30], Z.Y. Pei[11], M.Y. Qi[1,3], Y.Q. Qi[14], B.Q. Qiao[1,3], J.J. Qin[7], D. Ruffolo[30], V. Rulev[25], A. Sáiz[30], L. Shao[14], O. Shchegolev[25,31], X.D. Sheng[1,3], J.Y. Shi[1,3], H.C. Song[26], Yu.V. Stenkin[25,31], V. Stepanov[25], Y. Su[32], Q.N. Sun[8], X.N. Sun[27], Z.B. Sun[33], P.H.T. Tam[18], Z.B. Tang[6,7], W.W. Tian[2,17], B.D. Wang[1,3], C. Wang[33], H. Wang[8], H.G. Wang[11], J.C. Wang[29], J.S. Wang[28], L.P. Wang[22], L.Y. Wang[1,3], R.N. Wang[8], W. Wang[18], W. Wang[12], X.G. Wang[27], X.J. Wang[1,3], X.Y. Wang[10], Y. Wang[8], Y.D. Wang[1,3], Y.J. Wang[1,3], Y.P. Wang[1,2,3], Z.H. Wang[9], Z.X. Wang[20], Zhen Wang[28], Zheng Wang[1,3,6], D.M. Wei[13], J.J. Wei[13], Y.J. Wei[1,2,3], T. Wen[20], C.Y. Wu[1,3], H.R. Wu[1,3], S. Wu[1,3], W.X. Wu[8], X.F. Wu[13], S.Q. Xi[1,3], J. Xia[7,13], J.J. Xia[8], G.M. Xiang[2,15], D.X. Xiao[16], G. Xiao[1,3], H.B. Xiao[11], G.G. Xin[12], Y.L. Xin[8], Y. Xing[15], D.L. Xu[28], R.X. Xu[26], L. Xue[22], D.H. Yan[29], J.Z. Yan[13], C.W. Yang[9], F.F. Yang[1,3,6], J.Y. Yang[18], L.L. Yang[18], M.J. Yang[1,3], R.Z. Yang[7], S.B. Yang[20], Y.H. Yao[9], Z.G. Yao[1,3], Y.M. Ye[23], L.Q. Yin[1,3], N. Yin[22], X.H. You[1,3], Z.Y. You[1,2,3], Y.H. Yu[22], Q. Yuan[13], H.D. Zeng[13], T.X. Zeng[1,3,6], W. Zeng[20], Z.K. Zeng[1,2,3], M. Zha[1,3], X.X. Zhai[1,3], B.B. Zhang[10], H.M. Zhang[10], H.Y. Zhang[22], J.L. Zhang[17], J.W. Zhang[9], L.X. Zhang[11], Li Zhang[20], Lu Zhang[14], P.F. Zhang[20], P.P. Zhang[14], R. Zhang[7,13], S.R. Zhang[14], S.S. Zhang[1,3], X. Zhang[10], X.P. Zhang[1,3], Y.F. Zhang[8], Y.L. Zhang[1,3], Yi Zhang[1,13], Yong Zhang[1,3], B. Zhao[8], J. Zhao[1,3], L. Zhao[6,7], L.Z. Zhao[14], S.P. Zhao[13,22], F. Zheng[33], Y. Zheng[8], B. Zhou[1,3], H. Zhou[28], J.N. Zhou[15], P. Zhou[10], R. Zhou[9], X.X. Zhou[8], C.G. Zhu[22], F.R. Zhu[8], H. Zhu[17], K.J. Zhu[1,2,3,6] and X. Zuo[1,3]

[1]Key Laboratory of Particle Astrophyics & Experimental Physics Division & Computing Center, Institute of High Energy Physics, Chinese Academy of Sciences, 100049 Beijing, China.

[2]University of Chinese Academy of Sciences, 100049 Beijing, China.

[3]TIANFU Cosmic Ray Research Center, Chengdu, Sichuan, China.

[4]Dublin Institute for Advanced Studies, 31 Fitzwilliam Place, 2 Dublin, Ireland.

[5]Max-Planck-Institut for Nuclear Physics, P.O. Box 103980, 69029 Heidelberg, Germany.

[6]State Key Laboratory of Particle Detection and Electronics, China.

[7]University of Science and Technology of China, 230026 Hefei, Anhui, China.

[8]School of Physical Science and Technology & School of Information Science and Technology, Southwest Jiaotong University, 610031 Chengdu, Sichuan, China.

[9]College of Physics, Sichuan University, 610065 Chengdu, Sichuan, China.

[10]School of Astronomy and Space Science, Nanjing University, 210023 Nanjing, Jiangsu, China.

[11]Center for Astrophysics, Guangzhou University, 510006 Guangzhou, Guangdong, China.

[12]School of Physics and Technology, Wuhan University, 430072 Wuhan, Hubei, China.

[13]Key Laboratory of Dark Matter and Space Astronomy, Purple Mountain Observatory, Chinese Academy of Sciences, 210023 Nanjing, Jiangsu, China.

[14]Hebei Normal University, 050024 Shijiazhuang, Hebei, China.

[15]Key Laboratory for Research in Galaxies and Cosmology, Shanghai Astronomical Observatory, Chinese Academy of Sciences, 200030 Shanghai, China.

[16]Key Laboratory of Cosmic Rays (Tibet University), Ministry of Education, 850000 Lhasa, Tibet, China.

[17]National Astronomical Observatories, Chinese Academy of Sciences, 100101 Beijing, China.

[18]School of Physics and Astronomy & School of Physics (Guangzhou), Sun Yat-sen University, 519000 Zhuhai, Guangdong, China.

[19]Dipartimento di Fisica dell'Università di Napoli `Federico II", Complesso Universitario di Monte Sant'Angelo, via Cinthia, 80126 Napoli, Italy.

[20]School of Physics and Astronomy, Yunnan University, 650091 Kunming, Yunnan, China.

[21]Departement de Physique Nucleaire et Corpusculaire, Faculte de Sciences, Universite de Genève, 24 Quai Ernest Ansermet, 1211 Geneva, Switzerland.

[22]Institute of Frontier and Interdisciplinary Science, Shandong University, 266237 Qingdao, Shandong, China.

[23]Department of Engineering Physics, Tsinghua University, 100084 Beijing, China.

[24]School of Physics and Microelectronics, Zhengzhou University, 450001 Zhengzhou, Henan, China.

PoS(ICRC2021)350

[25]Institute for Nuclear Research of Russian Academy of Sciences, 117312 Moscow, Russia.
[26]School of Physics, Peking University, 100871 Beijing, China.
[27]School of Physical Science and Technology, Guangxi University, 530004 Nanning, Guangxi, China.
[28]Tsung-Dao Lee Institute & School of Physics and Astronomy, Shanghai Jiao Tong University, 200240 Shanghai, China.
[29]Yunnan Observatories, Chinese Academy of Sciences, 650216 Kunming, Yunnan, China.
[30]Department of Physics, Faculty of Science, Mahidol University, 10400 Bangkok, Thailand.
[31]Moscow Institute of Physics and Technology, 141700 Moscow, Russia.
[32]Key Laboratory of Radio Astronomy, Purple Mountain Observatory, Chinese Academy of Sciences, 210023 Nanjing, Jiangsu, China.
[33]National Space Science Center, Chinese Academy of Sciences, 100190 Beijing, China.